CHEMISTRY OF MATERIALS

pubs.acs.org/cm

Article

Pressure-Modulated Magnetism and Negative Thermal Expansion in the Ho_2Fe_{17} Intermetallic Compound

Yili Cao, Haowei Zhou, Sergii Khmelevskyi, Kun Lin, Maxim Avdeev, Chin-Wei Wang, Bingjie Wang, Fengxia Hu, Kenichi Kato, Takanori Hattori, Jun Abe, Koji Ohara, Saori Kawaguchi, Qiang Li, Masayuki Fukuda, Takumi Nishikubo, Koomok Lee, Takehiro Koike, Qiumin Liu, Jun Miao, Jinxia Deng, Baogen Shen, Masaki Azuma, and Xianran Xing*

Cite This: *Chem. Mater.* 2023, 35, 3249−3255

Read Online

ACCESS | Metrics & More | Article Recommendations | Supporting Information

ABSTRACT: Hydrostatic and chemical pressure are efficient stimuli to alter the crystal structure and are commonly used for tuning electronic and magnetic properties in materials science. However, chemical pressure is difficult to quantify and a clear correspondence between these two types of pressure is still lacking. Here, we study intermetallic candidates for a permanent magnet with a negative thermal expansion (NTE). Based on in situ synchrotron X-ray diffraction, negative chemical pressure is revealed in Ho_2Fe_{17} on Al doping and quantitatively evaluated by using temperature and pressure dependence of unit cell volume. A combination of magnetization and neutron diffraction measurements also allowed one to compare the effect of chemical pressure on magnetic ordering with that of hydrostatic pressure. Intriguingly, pressure can be used to control suppression and enhancement of NTE. Electronic structure calculations indicate that pressure affected the top of the majority band with respect to the Fermi level (E_F), which has implications for the magnetic stability, which in turn plays a critical role in modulating magnetism and NTE. This work presents a good example of understanding the effect of pressure and utilizing it to control properties of functional materials.

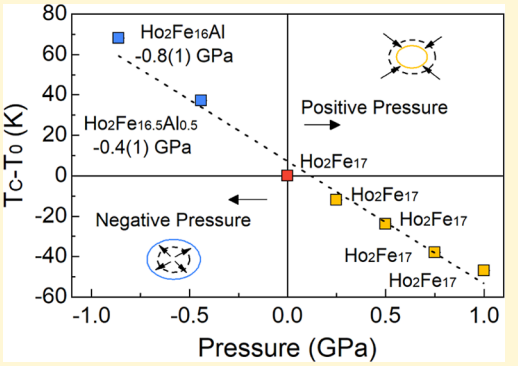

INTRODUCTION

Pressure as an efficient stimulus acting on lattices has aroused considerable interests in the context of tuning electronic and magnetic properties in materials science.[1] Apart from external hydrostatic pressure, chemical pressure is easier to realize via doping or interface constraint, and the effect can correspond to either positive or negative external pressure.[2] For example, negative chemical pressure emerges in epitaxial thin films of $PbTiO_3$/PbO and $BaTiO_3$/BaO due to interphase strain, leading to giant ferroelectric polarization and ordering temperature.[3,4] Nevertheless, understanding the mechanism of chemical pressure effects on properties remains a challenge. In comparison with physical pressure, the determination of chemical pressure is much more indirect and typically only qualitative. Bridging the connection between chemical and physical pressure thus remains an open issue.

Negative thermal expansion (NTE) is a peculiar physical phenomenon in solids,[5−8] which may originate from coupling between the lattice and spin and/or orbital degrees of freedom or from particular lattice dynamics, such as transverse phonon modes in flexible frameworks, such as ZrW_2O_8,[9] cyanides, and MOFs.[10−13] Other examples include spontaneous polarization in $PbTiO_3$ ferroelectric perovskites,[14] charge ordering in V_2OPO_4,[15] and magnetic transition in $Mn_3Cu_{0.5}Ge_{0.5}N$ and $La(Fe,Co,Si)_{13}$.[16,17] Unsurprisingly, the NTE is sensitive to lattice strain from pressure, which can be used for tuning the effect. For example, hydrostatic pressure applied to antiperovskite Mn_3GaN can weaken the thermal expansion anomaly via modifying magnetic interactions.[18] Positive chemical pressure induced in its analogue nanocrystalline $Mn_3Cu_{0.5}Ge_{0.5}N$ reduces NTE to zero.[19] Therefore, the NTE materials can be good model systems to establish the correspondence between physical and chemical pressure.

Here, we investigate the intermetallic candidate for a permanent magnet with NTE. In situ variable temperature and pressure synchrotron X-ray diffraction was used to quantitatively evaluate negative chemical pressure in Ho_2Fe_{17} with Al doping. Magnetization and neutron diffraction measurements were employed to understand the effect of chemical and hydrostatic pressure on magnetic ordering and

Received: January 23, 2023
Revised: March 26, 2023
Published: April 5, 2023

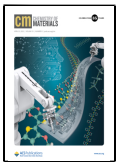

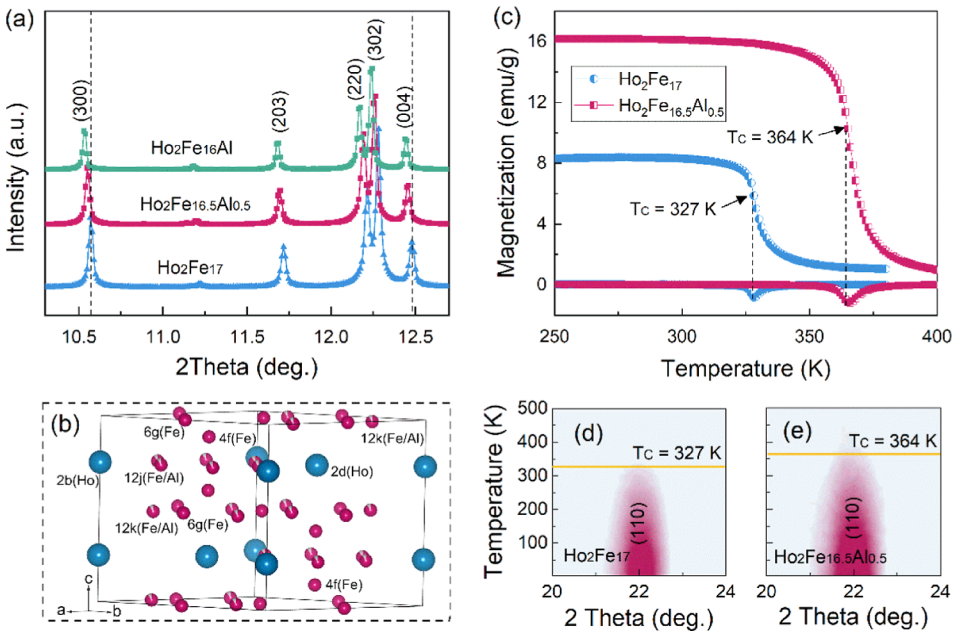

Figure 1. (a) SXRD patterns of $Ho_2Fe_{17-x}Al_x$ (x = 0, 0.5, 1.0) at room temperature; (b) crystal structure of $Ho_2(Fe,Al)_{17}$ determined by SXRD; (c) temperature dependence of magnetization for Ho_2Fe_{17} and $Ho_2Fe_{16.5}Al_{0.5}$, respectively; and (d) contour plot of NPD from 3 to 500 K for Ho_2Fe_{17} and (e) $Ho_2Fe_{16.5}Al_{0.5}$, respectively.

the resulting suppression and enhancement of NTE. First-principles calculations indicated that pressure shifts the top of the majority band, which plays a critical role in manipulating magnetism-driven NTE. This work explores the relationship between physical and chemical pressure and presents an example of using pressure to modify properties of functional materials.

MATERIALS AND METHODS

Sample Preparation. The $Ho_2(Fe,Al)_{17}$ intermetallic compounds were prepared by conventional arc-melting under a high purity argon atmosphere. The raw materials, Ho, Fe, and Al, were at least 99.9% purity. To ensure the chemical homogeneity, the ingots were re-melted at least 4 times and sealed in a quartz tube with high vacuum. Then, the quartz tube was annealed at 1373 K for 5 days and finally quenched into ice water. The ingots were ground into fine powder for powder diffraction and magnetic measurements.

Synchrotron X-ray Powder Diffraction. High-resolution synchrotron X-ray powder diffraction (SXRD) was conducted at a beamline BL44B2 of SPring-8, Japan (λ = 0.45 Å). High-pressure SXRD patterns were carried out at the beamline of BL10XU of Spring-8 Japan (λ = 0.42 Å) using a diamond anvil cell. To improve particle sampling statistics, the powder for the SXRD experiment was selected by a 600 mesh/in.^{2} sifter.

Neutron Powder Diffraction. High-resolution neutron powder diffraction (NPD) and magnetic field NPD of Ho_2Fe_{17} and $Ho_2Fe_{16.5}Al_{0.5}$ were obtained at ECHIDNA of the Australian Nuclear Science and Technology Organization (λ = 1.6215 Å) from 3 to 650 K. High-pressure NPD experiments were carried out at PLANET of J-PARC up to 300 K from 0 to +2.0(1) GPa (see the Supporting Information for details).[20] All the diffraction data was refined by Rietveld methods using FULLPROF package.[21]

Magnetization Experiments. Magnetization measurements were performed using Superconducting Quantum Interference Device (SQUID) and Physical Property Measurement System (PPMS) of Quantum Design. Magnetization as a function of temperature and applied magnetic field ($M-T$ & $M-H$) curves was measured. The hydrostatic pressures were performed up to +1.0 GPa by using the nonmagnetic BeCu cylindrical cell (Quantum Design).

Computational Method. To calculate the electronic structure of $Ho_2(Fe,Al)_{17}$ alloys with a substitutional atomic disorder we employ the Coherent Potential Approximation (CPA) in the framework of the Korringa–Kohn–Rostoker (KKR) band structure method and the Atomic Sphere Approximation (ASA).[22,23] In our KKR–ASA calculations, the partial wave functions were expanded in a spdf-basis (up to l = 3) and the effects of exchange and correlation are treated within the density functional theory using a Perdew–Wang[24] exchange–correlation functional. To model thermal magnetic disorder above the magnetic ordering temperature, we employ disordered local moment (DLM)[25] formalism based on the CPA. The choice of the ASA spheres on different crystallographic sites were made similar to our earlier works on $R_2(Fe,Co)_{17}$ alloys.[26]

RESULTS AND DISCUSSION

High-resolution SXRD patterns indicate all the as-prepared samples crystallize in a hexagonal cell (space group: $P6_3/mmc$), in which there are six non-equivalent Wyckoff sites: 2b (0, 0, 1/4), 2d (1/3, 2/3, 3/4), 4f (1/3, 2/3, z), 6g (1/2, 0, 0), 12j (x, y, 1/4), and 12k (x, 2x, z), respectively (Figure 1a,b). The careful structural refinements show the Al atoms occupy on the Fe-sublattice and show a preferred occupation on 12j and 12k sites in $Ho_2Fe_{16.5}Al_{0.5}$, consistent with that of our previous work on high Al content.[27] However, the a-axis lattice parameter expands from 8.45(1) of Ho_2Fe_{17} to 8.49(1) Å of $Ho_2Fe_{16}Al$, generating about 0.4% increase. A similar trend can also be observed in the c-axis lattice parameter (0.3% increase), which results in an almost isotropic expansion of unit cell volume, i.e., negative chemical pressure (Figure S1).

Although the Al is a non-magnetic element, the large lattice strain can bring about the change of the exchange interaction and hence adjust magnetic ordering. Ho_2Fe_{17} has been documented to be ferrimagnetic (FIM) below ~340 K.[28] Intriguingly, the magnetic ordering of $Ho_2Fe_{16.5}Al_{0.5}$ becomes more robust and magnetic ordering temperature increases up to 364 K (Figure 1c). In order to investigate the detailed magnetic structure, a temperature-dependent NPD experiment was carried out for $Ho_2Fe_{16.5}Al_{0.5}$ compounds (Figure 1d,e). It

https://doi.org/10.1021/acs.chemmater.3c00158
Chem. Mater. 2023, 35, 3249–3255

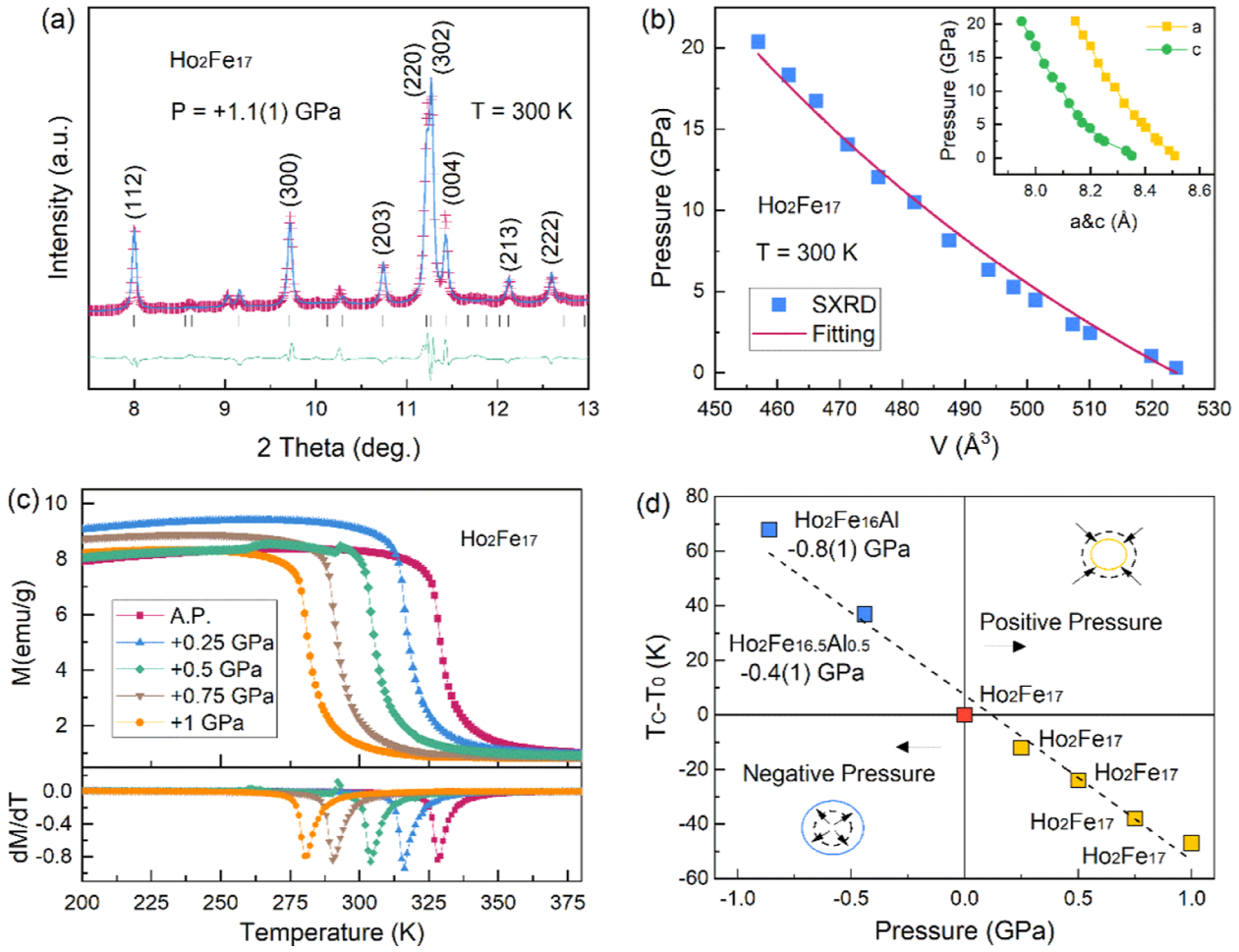

Figure 2. (a) SXRD patterns of Ho_2Fe_{17} at room temperature under +1.1(1) GPa; (b) pressure dependence of unit cell volume for Ho_2Fe_{17} at room temperature up to +20.4(1) GPa, the inset shows pressure dependence of lattice parameters *a* and *c*, respectively; (c) *M*−*T* curves and their differentials for Ho_2Fe_{17} under applying pressure of ambient pressure (A.P.), +0.25, +0.5, +0.75, and +1.0 GPa, respectively; and (d) correlation between $T_C - T_0$ and pressure, T_0 represents for the T_C of Ho_2Fe_{17} at ambient pressure.

was found that no extra magnetic reflections emerge below 380 K while the (110) peak intensity increases in the 2θ region around 22°. The FIM configuration is analyzed by the Rietveld method, with a model similar to that of Ho_2Fe_{17}, in which the magnetic moments of Ho and Fe atoms ($\mathbf{M}_{Ho}$ and $\mathbf{M}_{Fe}$) have an antiparallel alignment within the basal plane. However, the magnitudes of $\mathbf{M}_{Fe}$ are distinctly reduced at 3 K for $Ho_2Fe_{16.5}Al_{0.5}$ and the $\mathbf{M}_{Ho}$ tends to dominate the total magnetization (Figure. S2). This indicates the lattice strain affects the magnetism of $Ho_2(Fe,Al)_{17}$ compounds.

In order to explore the correlations between lattice strain and magnetic ordering in detail, the systematic variable pressure diffraction and magnetization experiments were carried out on Ho_2Fe_{17}. It was found that there was no any phase transition up to +20.4(1) GPa and all the reflections can be well indexed by the original hexagonal symmetry (Figure S3) and a representative Rietveld plot is shown in Figure 2a. The lattice contracts monotonically under pressure (Figure 2b). For example, the *a* and *c* are 8.51(0) and 8.35(0) Å at +0.3(0) GPa, respectively, and 8.15(1) and 7.95(0) Å at +20.4(1) GPa, respectively. Both *a* and *c* decrease by ∼ 4.2(3)% from +0.3(0) to +20.4(1) GPa, yielding a volumetric contraction ∼12.8(1) %. The resulting bulk elasticity modulus *K* determined by the first-order Murnaghan's equation of state is about 108 ± 2 GPa, which is similar to that of other Er_2Fe_{17} compounds.[29,30]

The *M*−*T* curves measured upon applying pressure from 0 to 1 GPa for Ho_2Fe_{17} are shown in Figure 2c. With the pressure increasing, the magnetic ordering is gradually weakened and the T_C decreases accordingly. For example, the T_C is reduced from 328 K at 0 GPa to 280 K at 1 GPa. This can also be evidenced in the pressure dependence NPD patterns, where it can be seen that the magnetic intensities, e.g., (112), vanish between +0.3 (1) and +0.7(1) GPa (Figures S4 and S5). By using the relative volumetric change derived from Al doping the negative chemical pressure of $Ho_2Fe_{16.5}Al_{0.5}$ and $Ho_2Fe_{16}Al$ can be well calculated according to the following equation

$$dP = -K \times dV/V_0 \quad (1)$$

in which, dP, dV/V_0, and K represent chemical pressure change, relative volume variation, and bulk elasticity modulus, respectively. To exclude the magnetic contribution, the unit cell volume at 450 K is used for this chemical pressure determination (Figure S6). Thereby, the negative chemical pressure is quantitatively evaluated to be −0.4 (1) and −0.8(1) GPa, for $Ho_2Fe_{16.5}Al_{0.5}$ and $Ho_2Fe_{16}Al$, respectively. Interestingly, the comparison of lattice strain with the T_C indicates a

https://doi.org/10.1021/acs.chemmater.3c00158
Chem. Mater. 2023, 35, 3249−3255

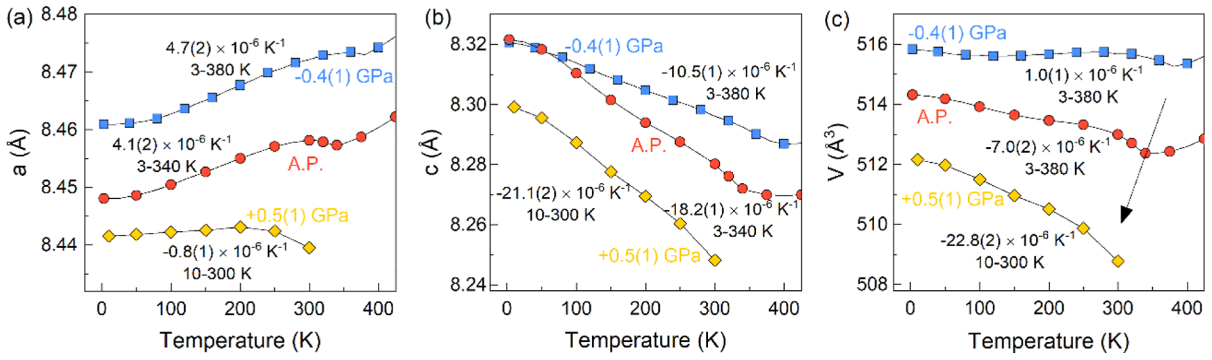

Figure 3. Effect of pressure on NTE. (a) Thermal expansion of Ho_2Fe_{17} at variable pressures of −0.4(1) GPa ($Ho_2Fe_{16.5}Al_{0.5}$), ambient pressure and +0.5(1) GPa along *a*, (b) *c* directions, and (c) unit cell volume *V*, respectively.

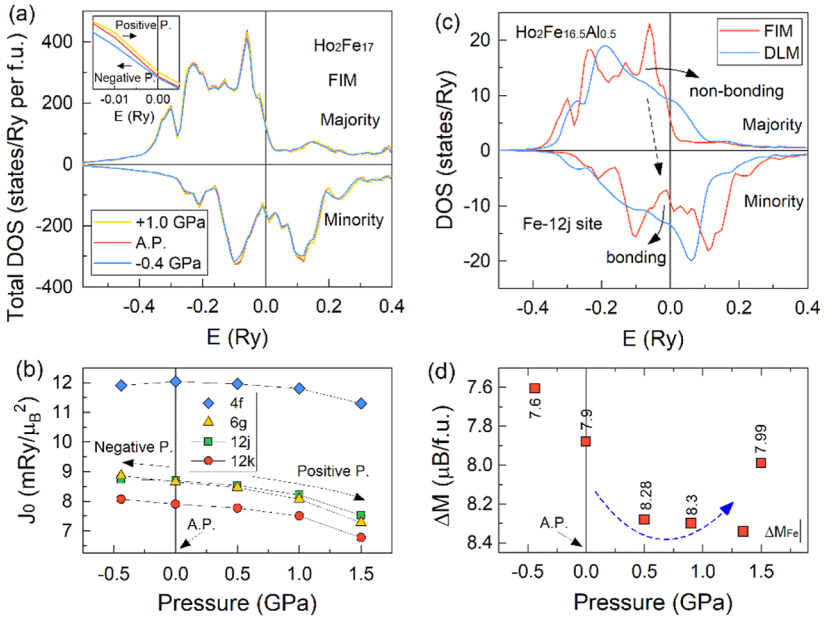

Figure 4. (a) Total DOS under FIM ordering for Ho_2Fe_{17} as a function of pressure, the inset shows the enlarged region; (b) molecular fields acting on the Fe-sublattice determined by electronic structure calculations at each site with pressure for Ho_2Fe_{17}; (c) atomic resolved contribution to the DOS under FIM and DLM at the Fe 12 j site for $Ho_2Fe_{16.5}Al_{0.5}$; and (d) difference of calculated M_{Fe} ($\Delta M = M_{Fe(FIM)} - M_{Fe(DLM)}$) as a function of pressure for Ho_2Fe_{17}.

strong effect of pressure on magnetic ordering in Ho_2Fe_{17} (Figure 2d).

Variable temperature structure analysis against NPD patterns was subsequently done for Ho_2Fe_{17} to investigate the evolution of NTE below T_C with pressure. The analysis revealed that there was no obvious structural transition over the whole investigated temperature range. As shown in Figure 3a−c, Ho_2Fe_{17} demonstrates anisotropic thermal expansion at ambient pressure: *a* exhibits low positive thermal expansion (PTE, $\bar{\alpha}_a = 4.1(2) \times 10^{-6}$ K^{-1}, 3−340 K) and *c* exhibits strong NTE ($\bar{\alpha}_c = -18.2(3) \times 10^{-6}$ K^{-1}, 3−340 K). Intriguingly, negative chemical pressure weakens the NTE along the *c* direction with little Al doping and gradually suppresses the volumetric NTE to zero, $\bar{\alpha}_V = -0.99 \times 10^{-6}$ K^{-1} (3−380 K) in $Ho_2Fe_{16.5}Al_{0.5}$, and the moderate PTE in $Ho_2Fe_{16}Al$ ($\bar{\alpha}_V = 3.63 \times 10^{-6}$ K^{-1}, 125−400 K). In contrast, the PTE of *a* axis is suppressed on applying hydrostatic pressure and thus, the magnitudes of volumetric NTE (10−300 K) can be enhanced (Figure S11). The largest NTE is observed under 0.5(1) GPa with $\alpha_V = -22.8(2) \times 10^{-6}$ K^{-1} (10−300 K), which is almost 3 times as large as that of ambient pressure because lattice parameter *a* stays almost constant under +0.5(1) GPa up to 300 K with $\bar{\alpha}_a = -0.8(1) \times 10^{-6}$ K^{-1} (10−300 K).

In order to fundamentally understand pressure-tuned magnetic ordering, electronic structure calculations were carried out on Ho_2Fe_{17} with different pressures. As shown in Figure 4a, the splitting of total density of state (DOS) occurs between the majority and minority bands due to strong spontaneous FIM ordering. The top of majority band locates near the E_F and is easily shifted by and pressure, which has implication for the magnetic stability and hence magnetic ordering. The negative pressure leads to the increasing of the molecular field acting on Fe sites in the ordered states as it is followed from our ab-initio calculation of the total exchange interaction constants, J_0, for different Fe sites at different volumes (Figure 4b). The respective J_0 constants have been calculated by employing the Green function-based magnetic-force theorem[31] embedded[32] in KKR−ASA formalism. Because the overlap of d-orbitals could be weakened with lattice expansion derived from the negative pressure,[33] the 3d electrons become more localized, which stabilizes the magnetic ordering with a higher total molecular field (Figure 4b).

https://doi.org/10.1021/acs.chemmater.3c00158
Chem. Mater. 2023, 35, 3249−3255

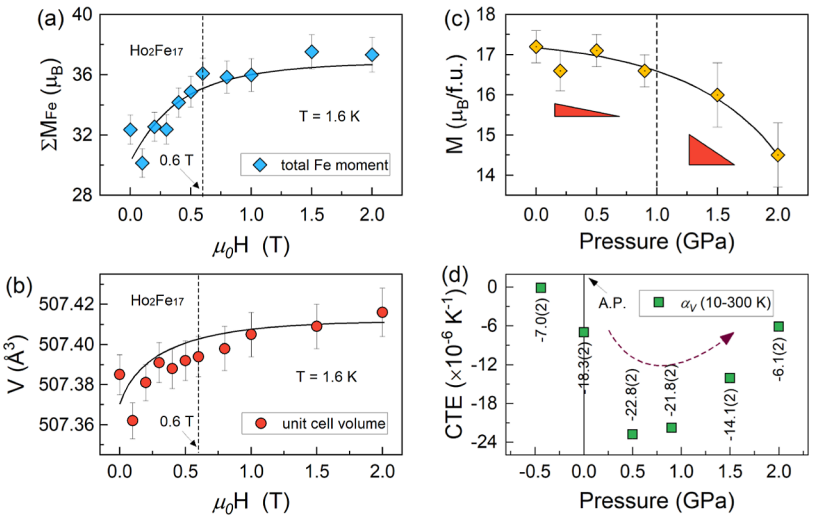

Figure 5. (a) Relative change of total magnetic Fe moments and (b) unit cell volume as a function of applied magnetic field for Ho_2Fe_{17} at 1.6 K; and (c) magnetic moments of Fe-sublattice at 10 K as a function of pressure up to +2.0(1) GPa; (d) the CTE (10−300 K) as a function of pressure up to +2.0(1) GPa for Ho_2Fe_{17}.

Thereby, the T_C increases as the top of the majority 3d band slightly shifts upward in energy below E_F. In contrast, positive pressure leads to band broadening and thus reduces the DOS at the E_F, which reduces the T_C accordingly.

Our calculations employed the disordered local moment (DLM) approach that is used to model the a high-temperature paramagnetic state,[25] identify that repopulation of the d-orbitals compare to the ordered FM state intimately occurs with different bonding states near the Fermi level (E_F), similar to other magnetic NTE systems, such as Fe−Ni,[23] Fe−Pt,[34] and Fe−Pd.[35] This process is schematically shown by the arrows in Figure 4c. The precise analysis of the bonding character of the states in Ho_2Fe_{17} is much more involved than in the simple case of the cubic Invar alloys like Fe−Ni (see details, e.g., in ref 36), due to a lower symmetry of the Fe sites. However, the main feature of the process can be well understood by the analogy. The nonbonding states are located at the top portion of the d-DOS having higher energy than metallic bonding states at lower energies. These nonbonding states become partially occupied only due to exchange splitting of the bands and some portion of the bonding state left unoccupied. For Fe in an ideal face-centered cubic (fcc) structure, there is exactly two nonbonding states per spin channel, e_g, at the top of the d-band. The nearest neighboring atomic shell of the position 4f Fe in Ho_2Fe_{17} may be regarded to have a similar but slightly distorted fcc environment, from which we can draw an analogy presented by arrows in Figure 4c. Note that the other Fe positions in Ho_2Fe_{17} are less coordinated, signaling that their contribution to the magneto-volume effect is less significant because they have more nonbonding states at the top of the d-band. In the paramagnetic state, local moments of Fe-sublattice can significantly decrease that affects the lattice change upon magnetic ordering (Figure 4d, Tables S7−S9). The change of local moment upon magnetic ordering is calculated at different pressures as $\Delta\mathbf{M} = \mathbf{M}_{FIM} - \mathbf{M}_{PM(DLM)}$. As a result of the pressure-induced shift in the position of the top of the d-band with respect to E_F, the local moment of the Fe sublattice can be delicately tuned. As a result, the magnetoelastic coupling can be controlled and in turn can be used to control the thermal expansion.

As shown in Figure 5a, magnetic field dependence of NPD well evidences such magnetic instability in Ho_2Fe_{17}, i.e., the magnetic moments keep increasing up to saturation near 0.6 T, and unit cell volume increases with the same trend (Figure 5b). On negative pressure, the magnetic ordering becomes more stable and the $\Delta\mathbf{M}$ decreases accordingly. The CTE turns from negative to zero and to positive with higher T_C. In contrast, positive pressure produces an opposite trend (Figure 5d). The magnetic moments show slight change up to +0.9(1) GPa, which leads to larger $\Delta\mathbf{M}$ between the FIM and DLM, resulting in stronger NTE. At higher pressure, the magnetic ordering dramatically weakens and the magnetic moment decreases accordingly (Figure 5c), whereby attenuating the $\Delta\mathbf{M}$ and the NTE. The CTE increases up to $\bar{\alpha}_V \sim -14.1(1)$ at +1.5(1) GPa (10−300 K), and $-6.1(2) \times 10^{-6}$ K^{-1} at +2.0(1) GPa, respectively. Overall, pressure enables not only ZTE but also unconventionally enhanced NTE in Ho_2Fe_{17}, which is rarely observed among magnetic NTE systems.[37]

CONCLUSIONS

In summary, systematic experimental and theoretical investigations were done to probe the effect on physical and chemical pressures on magnetism and NTE in Ho_2Fe_{17} and Al-doped $Ho_2Fe_{16.5}Al_{0.5}$. Negative chemical pressure emerging in Ho_2Fe_{17} on Al doping was quantified by comparing temperature and pressure dependence of unit cell volume with those in Ho_2Fe_{17} under external pressure. As a result, the consistent picture of the effect of chemical and hydrostatic pressure on magnetic ordering is revealed. Intriguingly, it was found that pressure can be used to suppress and enhance the NTE. The pressure-induced shift of the top of the majority band with respect to the Fermi level (E_F) has implications for the magnetic stability, which plays a critical role in modulating magnetism and NTE. These findings demonstrate how chemical pressure, either in bulk via chemical doping or interfaces via lattice mismatch, can be used to control magnetism-driven NTE.

https://doi.org/10.1021/acs.chemmater.3c00158
Chem. Mater. 2023, 35, 3249−3255

■ ASSOCIATED CONTENT

Supporting Information

The Supporting Information is available free of charge at https://pubs.acs.org/doi/10.1021/acs.chemmater.3c00158.

Refinement of diffraction data and relevant results of electronic structure calculations (PDF)

■ AUTHOR INFORMATION

Corresponding Author

Xianran Xing − *Beijing Advanced Innovation Center for Materials Genome Engineering, Institute of Solid State Chemistry, University of Science and Technology Beijing, Beijing 100083, China;* orcid.org/0000-0003-0704-8886; Email: xing@ustb.edu.cn

Authors

Yili Cao − *Beijing Advanced Innovation Center for Materials Genome Engineering, Institute of Solid State Chemistry, University of Science and Technology Beijing, Beijing 100083, China*

Haowei Zhou − *Beijing Advanced Innovation Center for Materials Genome Engineering, Institute of Solid State Chemistry, University of Science and Technology Beijing, Beijing 100083, China*

Sergii Khmelevskyi − *Research Center for Computational Materials Science and Engineering, Vienna University of Technology, Vienna A-1040, Austria*

Kun Lin − *Beijing Advanced Innovation Center for Materials Genome Engineering, Institute of Solid State Chemistry, University of Science and Technology Beijing, Beijing 100083, China;* orcid.org/0000-0003-4515-3206

Maxim Avdeev − *Australian Nuclear Science and Technology Organisation, Lucas Heights, New South Wales 2234, Australia; School of Chemistry, The University of Sydney, Sydney, New South Wales 2006, Australia;* orcid.org/0000-0003-2366-5809

Chin-Wei Wang − *Neutron Group, National Synchrotron Radiation Research Center, Hsinchu 30076, Taiwan*

Bingjie Wang − *Beijing National Laboratory for Condensed Matter Physics, Institute of Physics, Chinese Academy of Sciences, Beijing 100190, China*

Fengxia Hu − *Beijing National Laboratory for Condensed Matter Physics, Institute of Physics, Chinese Academy of Sciences, Beijing 100190, China;* orcid.org/0000-0003-0383-0213

Kenichi Kato − *RIKEN SPring-8 Center, Hyogo 679-5148, Japan*

Takanori Hattori − *J-PARC Center, Japan Atomic Energy Agency (JAEA), Tokai, Ibaraki 319-1195, Japan*

Jun Abe − *Neutron Science and Technology Center, Comprehensive Research Organization for Science and Society (CROSS), Tokai, Ibaraki 319-1106, Japan*

Koji Ohara − *SPring-8, Japan Synchrotron Radiation Research Institute, Hyogo 679-5148, Japan;* orcid.org/0000-0002-3134-512X

Saori Kawaguchi − *SPring-8, Japan Synchrotron Radiation Research Institute, Hyogo 679-5148, Japan*

Qiang Li − *Beijing Advanced Innovation Center for Materials Genome Engineering, Institute of Solid State Chemistry, University of Science and Technology Beijing, Beijing 100083, China;* orcid.org/0000-0003-4259-6984

Masayuki Fukuda − *Laboratory for Materials and Structures, Tokyo Institute of Technology, Yokohama 226-8503, Japan*

Takumi Nishikubo − *Laboratory for Materials and Structures, Tokyo Institute of Technology, Yokohama 226-8503, Japan;* orcid.org/0000-0002-1250-3057

Koomok Lee − *Laboratory for Materials and Structures, Tokyo Institute of Technology, Yokohama 226-8503, Japan*

Takehiro Koike − *Laboratory for Materials and Structures, Tokyo Institute of Technology, Yokohama 226-8503, Japan;* orcid.org/0000-0002-3588-6708

Qiumin Liu − *Laboratory for Materials and Structures, Tokyo Institute of Technology, Yokohama 226-8503, Japan*

Jun Miao − *Beijing Advanced Innovation Center for Materials Genome Engineering, Institute of Solid State Chemistry, University of Science and Technology Beijing, Beijing 100083, China;* orcid.org/0000-0002-6924-0737

Jinxia Deng − *Beijing Advanced Innovation Center for Materials Genome Engineering, Institute of Solid State Chemistry, University of Science and Technology Beijing, Beijing 100083, China*

Baogen Shen − *Beijing National Laboratory for Condensed Matter Physics, Institute of Physics, Chinese Academy of Sciences, Beijing 100190, China;* orcid.org/0000-0003-4819-1806

Masaki Azuma − *Laboratory for Materials and Structures, Tokyo Institute of Technology, Yokohama 226-8503, Japan;* orcid.org/0000-0002-8378-321X

Complete contact information is available at: https://pubs.acs.org/10.1021/acs.chemmater.3c00158

Notes

The authors declare no competing financial interest.

■ ACKNOWLEDGMENTS

This research was supported by National Key R&D Program of China (2020YFA0406202) and National Natural Science Foundation of China (22090042, 22275015, 21731001, and 21971009). The synchrotron radiation experiments were conducted at the BL44B2 and BL10XU of SPring-8 with the approval of the Japan Synchrotron Radiation Research Institute (JASRI) (Proposal nos. 2023A1351 and 2021B1195). Neutron diffraction experiments were carried out on ECHIDNA in the Australian Nuclear Science and Technology Organization (ANSTO) and PLANET in the J-PARC (Proposal nos. 2021I0011 and 2021B0409).

■ REFERENCES

(1) Lin, K.; Li, Q.; Yu, R.; Chen, J.; Attfield, J. P.; Xing, X. Chemical pressure in functional materials. *Chem. Soc. Rev.* **2022**, *51*, 5351−5364.

(2) Park, J.; Hwang, J.-Y.; Lee, K. H.; Kim, S.-G.; Lee, K.; Kim, S. W. Tuning the spin-alignment of interstitial electrons in two-dimensional Y_2C electride via chemical pressure. *J. Am. Chem. Soc.* **2017**, *139*, 17277−17280.

(3) Zhang, L.; Chen, J.; Fan, L.; Diéguez, O.; Cao, J.; Pan, Z.; Wang, Y.; Wang, J.; Kim, M.; Deng, S.; et al. Giant polarization in super-tetragonal thin films through interphase strain. *Science* **2018**, *361*, 494−497.

(4) Wang, Y.; Zhang, L.; Wang, J.; Li, Q.; Wang, H.; Gu, L.; Chen, J.; Deng, J.; Lin, K.; Huang, L.; et al. Chemical-Pressure-Modulated $BaTiO_3$ Thin Films with Large Spontaneous Polarization and High Curie Temperature. *J. Am. Chem. Soc.* **2021**, *143*, 6491−6497.

(5) Mary, T. A.; Evans, J. S. O.; Vogt, T.; Sleight, A. W. Negative thermal expansion from 0.3 to 1050 Kelvin in ZrW_2O_8. *Science* **1996**, *272*, 90−92.
(6) Goodwin, A. L.; Calleja, M.; Conterio, M. J.; Dove, M. T.; Evans, J. S. O.; Keen, D. A.; Peters, L.; Tucker, M. G. Colossal positive and negative thermal expansion in the framework material $Ag_3[Co(CN)_6]$. *Science* **2008**, *319*, 794−797.
(7) Takenaka, K.; Takagi, H. Zero thermal expansion in a pure-form antiperovskite manganese nitride. *Appl. Phys. Lett.* **2009**, *94*, 131904.
(8) Greve, B. K.; Martin, K. L.; Lee, P. L.; Chupas, P. J.; Chapman, K. W.; Wilkinson, A. P. Pronounced negative thermal expansion from a simple structure: cubic ScF_3. *J. Am. Chem. Soc.* **2010**, *132*, 15496−15498.
(9) Ernst, G.; Broholm, C.; Kowach, G. R.; Ramirez, A. P. Phonon density of states and negative thermal expansion in ZrW_2O_8. *Nature* **1998**, *396*, 147−149.
(10) Gallington, L. C.; Chapman, K. W.; Morelock, C. R.; Chupas, P. J.; Wilkinson, A. P. Dramatic softening of the negative thermal expansion material HfW_2O_8 upon heating through its WO_4 orientational order-disorder phase transition. *J. Appl. Phys.* **2014**, *115*, 053512.
(11) Morelock, C. R.; Gallington, L. C.; Wilkinson, A. P. Solid solubility, phase transitions, thermal expansion, and compressibility in $Sc_{1-x}Al_xF_3$. *J. Solid State Chem.* **2015**, *222*, 96−102.
(12) Chapman, K. W.; Chupas, P. J. Pressure enhancement of negative thermal expansion behavior and induced framework softening in zinc cyanide. *J. Am. Chem. Soc.* **2007**, *129*, 10090−10091.
(13) Liu, Z.; Gao, Q.; Chen, J.; Deng, J.; Lin, K.; Xing, X. Negative thermal expansion in molecular materials. *Chem. Commun.* **2018**, *54*, 5164−5176.
(14) Chen, J.; Hu, L.; Deng, J.; Xing, X. Negative thermal expansion in functional materials: controllable thermal expansion by chemical modifications. *Chem. Soc. Rev.* **2015**, *44*, 3522−3567.
(15) Pachoud, E.; Cumby, J.; Lithgow, C. T.; Attfield, J. P. Charge order and negative thermal expansion in V_2OPO_4. *J. Am. Chem. Soc.* **2018**, *140*, 636−641.
(16) Kodama, K.; Iikubo, S.; Takenaka, K.; Takigawa, M.; Takagi, H.; Shamoto, S. Gradual development of Γ^{5g} antiferromagnetic moment in the giant negative thermal expansion material $Mn_3Cu_{1-x}Ge_xN$ ($x \sim 0.5$). *Phys. Rev. B* **2010**, *81*, 224419.
(17) Huang, R.; Liu, Y.; Fan, W.; Tan, J.; Xiao, F.; Qian, L.; Li, L. Giant negative thermal expansion in $NaZn_{13}$-type $La(Fe,Si,Co)_{13}$ compounds. *J. Am. Chem. Soc.* **2013**, *135*, 11469−11472.
(18) Shi, K.; Sun, Y.; Yan, J.; Deng, S.; Wang, L.; Wu, H.; Hu, P.; Lu, H.; Malik, M. I.; Huang, Q.; et al. Baromagnetic Effect in Antiperovskite $Mn_3Ga_{0.95}N_{0.94}$ by Neutron Powder Diffraction Analysis. *Adv. Mater.* **2016**, *28*, 3761−3767.
(19) Song, X.; Sun, Z.; Huang, Q.; Rettenmayr, M.; Liu, X.; Seyring, M.; Li, G.; Rao, G.; Yin, F. Adjustable Zero Thermal Expansion in Antiperovskite Manganese Nitride. *Adv. Mater.* **2011**, *23*, 4690−4694.
(20) Aso, N.; Fujiwara, T.; Uwatoko, Y.; Miyano, H.; Yoshizawa, H. Development of a hybrid CuBe/NiCrAl clamp-type high pressure cell for neutron diffraction. *J. Phys. Soc. Jpn.* **2007**, *76*, 228−229.
(21) Rodríguez-Carvajal, J. *FullProf*; CEA/Saclay: France, 2001.
(22) Abrikosov, I. A.; Skriver, H. L. Self-consistent linear-muffin-tin-orbitals coherent-potential technique for bulk and surface calculations: Cu-Ni, Ag-Pd, and Au-Pt random alloys. *Phys. Rev. B* **1993**, *47*, 16532−16541.
(23) Ruban, A. V.; Khmelevskyi, S.; Mohn, P.; Johansson, B. Magnetic state, magnetovolume effects, and atomic order in $Fe_{65}Ni_{35}$ Invar alloy: A first principles study. *Phys. Rev. B* **2007**, *76*, 014420.
(24) Perdew, J. P.; Wang, Y. Accurate and simple analytic representation of the electron-gas correlation energy. *Phys. Rev. B* **1992**, *45*, 13244−13249.
(25) Gyorffy, B. L.; Pindor, A. J.; Staunton, J.; Stocks, G. M.; Winter, H. A first-principles theory of ferromagnetic phase transitions in metals. *J. Phys. F: Met. Phys.* **1985**, *15*, 1337−1386.
(26) Cao, Y.; Lin, K.; Khmelevskyi, S.; Avdeev, M.; Taddei, K. M.; Zhang, Q.; Huang, Q.; Li, Q.; Kato, K.; Tang, C. C.; et al. Ultrawide Temperature Range Super-Invar Behavior of $R_2(Fe,Co)_{17}$ Materials (R = Rare Earth). *Phys. Rev. Lett.* **2021**, *127*, 055501.
(27) Cao, Y.; Lin, K.; Liu, Z.; Hu, J.; Wang, C.-W.; Avdeev, M.; Li, Q.; Deng, J.; Chen, J.; Zhang, H.; et al. Neutron diffraction study of unusual magnetic behaviors in the $Ho_2Fe_{11}Al_6$ intermetallic compound. *Inorg. Chem.* **2019**, *58*, 13742−13745.
(28) Wang, J. L.; Studer, A. J.; Kennedy, S. J.; Zeng, R.; Dou, S. X.; Campbell, S. J. Magnetovolume effect in $Ho_2Fe_{17-x}Mn_x$ compounds. *J. Appl. Phys.* **2012**, *111*, 07A911.
(29) Alvarez-Alonso, P.; Gorria, P.; Blanco, J. A.; Sánchez-Marcos, J.; Cuello, G. J.; Puente-Orench, I.; Rodríguez-Velamazán, J. A.; Garbarino, G.; De Pedro, I.; Fernández, J. R.; et al. Magnetovolume and magnetocaloric effects in Er_2Fe_{17}. *Phys. Rev. B* **2012**, *86*, 184411.
(30) Arnold, Z.; Kamarád, J.; Prokhnenko, O.; Ritter, C.; Eto, T.; Honda, F.; Oomi, G.; García-Landa, B. Anisotropy of Linear Thermal Expansion and Compressibility of Y_2Fe_{17} Under Pressure and its Correlation to Magnetic Structure. *High Pressure Res.* **2002**, *22*, 175−179.
(31) Liechtenstein, A. I.; Katsnelson, M.; Antropov, V.; Gubanov, V. Local spin density functional approach to the theory of exchange interactions in ferromagnetic metals and alloys. *J. Magn. Magn. Mater.* **1987**, *67*, 65−74.
(32) Ruban, A. V.; Simak, S. I.; Shallcross, S.; Skriver, H. L. Local lattice relaxations in random metallic alloys: Effective tetrahedron model and supercell approach. *Phys. Rev. B* **2003**, *67*, 214302.
(33) Takenaka, K. Progress of research in negative thermal expansion materials: paradigm shift in the control of thermal expansion. *Front. Chem.* **2018**, *6*, 267.
(34) Khmelevskyi, S.; Ruban, A. V.; Kakehashi, Y.; Mohn, P.; Johansson, B. Ab initio investigation of the Invar anomaly in ordered fcc Fe-Pt alloys. *Phys. Rev. B* **2005**, *72*, 064510.
(35) Winterrose, M. L.; Lucas, M. S.; Yue, A. F.; Halevy, I.; Mauger, L.; Muñoz, J. A.; Hu, J.; Lerche, M.; Fultz, B. Pressure-induced invar behavior in Pd_3Fe. *Phys. Rev. Lett.* **2009**, *102*, 237202.
(36) Entel, P.; Hoffmann, E.; Mohn, P.; Schwarz, K.; Moruzzi, V. L. First-principles calculations of the instability leading to the Invar effect. *Phys. Rev. B* **1993**, *47*, 8706−8720.
(37) Salvador, J. R.; Guo, F.; Hogan, T.; Kanatzidis, M. G. Zero thermal expansion in YbGaGe due to an electronic valence transition. *Nature* **2003**, *425*, 702−705.

https://doi.org/10.1021/acs.chemmater.3c00158
Chem. Mater. 2023, 35, 3249−3255